Diffusive Escape of a Nanoparticle from a Porous Cavity

Dapeng Wang,[1,2,*] Haichao Wu,[2,*] Lijun Liu,[1] Jizhong Chen,[1,†] and Daniel K. Schwartz[2,‡]
[1]State Key Laboratory of Polymer Physics and Chemistry, Changchun Institute of Applied Chemistry, Chinese Academy of Sciences, Changchun 130022, Peoples Republic of China
[2]Department of Chemical and Biological Engineering, University of Colorado Boulder, Boulder, Colorado 80309, USA

(Received 9 January 2019; revised manuscript received 26 April 2019; published 11 September 2019)

Narrow escape from confinement through a nanochannel is the critical step of complex transport processes including size-exclusion-based separations, oil and gas extraction from the microporous subsurface environment, and ribonucleic acid translocation through nuclear pore complex channels. While narrow escape has been studied using theoretical and computational methods, experimental quantification is rare because of the difficulty in confining a particle into a microscopic space through a nanoscale hole. Here, we studied narrow escape in the context of continuous nanoparticle diffusion within the liquid-filled void space of an ordered porous material. Specifically, we quantified the spatial dependence of nanoparticle motion and the sojourn times of individual particles in the interconnected confined cavities of a liquid-filled inverse opal film. We found that nanoparticle motion was inhibited near cavity walls and cavity escape was slower than predicted by existing theories and random-walk simulations. A combined computational-experimental analysis indicated that translocation through a nanochannel is barrier controlled rather than diffusion controlled.

DOI: 10.1103/PhysRevLett.123.118002

In the absence of confining interfaces, the mean-square displacement (MSD) of Brownian motion grows linearly over time and the corresponding displacement is Gaussian distributed [1,2]. This simple picture breaks down within tortuous interconnected porous environments, where the internal geometry of void spaces can confine diffusion [3–5]. Observing spatially confined diffusional trajectories can potentially provide information about the local microstructure [6–14]. Moreover, confinement can fundamentally change the statistics of Brownian motion via, e.g., transient adsorption or desorption [15,16], particle-wall interactions [17,18], entropic [19,20] or hydrodynamic [21,22] effects, and other noncovalent interactions. These effects cause deviations from Brownian motion, manifesting as a range of anomalous behavior, such as obstructed slow transport, nonlinear MSD, and/or non-Gaussian-distributed displacements. Notably, recent observations suggested that the accessible volume explored by a particle in heterogeneous porous materials was smaller than expected [23–25]; the underlying mechanisms are not yet understood.

The rate-determining factor of limited accessibility is the narrow escape through bottlenecks within porous void spaces. To study the origin of the transport mechanism, a straightforward approach is to quantify the sojourn time in a well-defined confined cavity prior to escape. A successful escape event consists of two naturally decoupled steps [26]: (1) the search for an opening, and (2) the subsequent translocation of a particle through the opening. The former is connected to the mathematical "narrow escape problem" that calculates the mean first passage time (MFPT) of a Brownian particle to an opening on a reflecting boundary of a confined domain. The current understanding of the latter is that the passage is controlled by a diffusion-limited barrier [23]. A variety of theoretical frameworks have been proposed that allow asymptotic evaluation of MFPT in various physical scenarios [27–38]; however, it remains challenging to test theoretical predictions experimentally. A pioneering "pore-cavity-pore" device represented an important first step to characterize the narrow escape problem [39].

Here, we experimentally study the escape of individual fluorescent polystyrene nanoparticles from a confined silica cavity in an index-matched solution consisting of thiodiethanol and the surfactant Triton X-100. The confined space comprises a silica inverse opal film consisting of a hexagonally close-packed interconnected network of spherical cavities, where each cavity has twelve circular holes that connect to adjacent cavities [40]. The holes allow the escape of a Brownian particle from one cavity to another, exploiting passive diffusion. We employed a multiplexed 3D single-particle imaging approach to record the sojourn time in a given cavity by identifying consecutive escape events of many particles simultaneously. This fully 3D tracking capability allowed us to address the "many-window escape problem" [32,34].

The silica inverse opals were prepared by evaporative deposition of monodisperse polystyrene spheres [40,41]. The resulting structure contained a high-quality silica inverse opal layer with extremely uniform cavity size over macroscopic length scales [Figs. 1(a) and 1(b)].

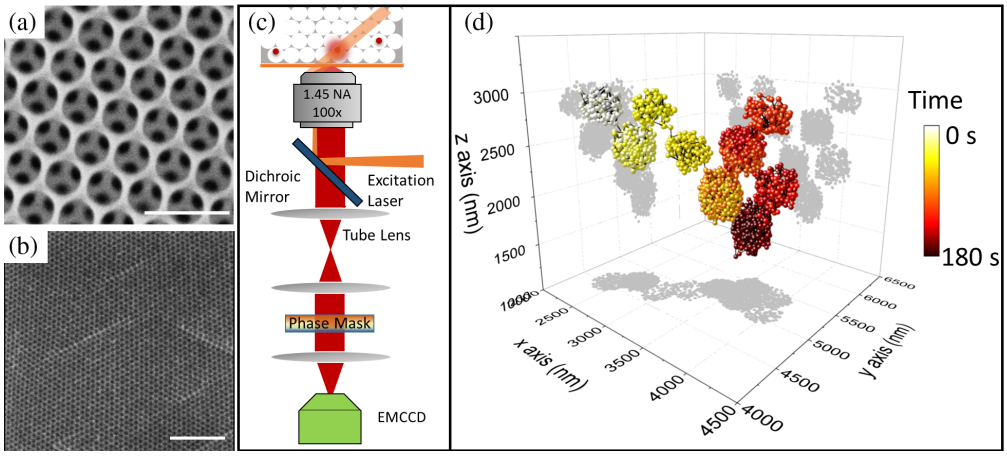

FIG. 1. (a) Representative scanning electron microscope image of an inverse opal film. The scale bar represents 1 μm. (b) Confocal laser scanning microscopy image of an inverse opal film filled with rhodamine 6G solution. The scale bar represents 5 μm. (c) A variable-angle wide-field microscope body was equipped with a phase mask that enabled double-helix point spread function imaging. (d) A representative 3D trajectory of a particle confined in an inverse opal structure.

The resulting structure had a cavity radius $R = 0.25$ μm and an adjustable hole diameter L that was controlled by varying the concentration of the silicate precursor solution (Fig. S2). The particles (hydrodynamic radius of 24 nm) were dispersed in a 1:5 mixture of thiodiethanol and Triton X-100 at a concentration of approximately 10^{-13}–$10^{-14}M$. This particular formulation was chosen because it simultaneously matched the refractive index of silica, minimized particle adhesion to the interior silica surfaces, and was sufficiently viscous to permit highly resolvable observations of particle motion. As such, the solution (while not commonly found in natural porous environments) served as an appropriate model system for observing confined nanoparticle mobility.

Some particles diffused passively and spontaneously into the interior void space. However, even under optimized conditions, a small fraction of particles were immobilized and accumulated over the course of the experiment, due to the presence of various attractive interactions (Table S1) and the fact that nanoparticle samples often exhibit surface heterogeneity [42,43]. While particle immobilization and retention is important in its own right, here we focused on the mobile nanoparticle population. We employed a 3D single-molecule imaging approach, which combined variable-angle illumination epifluorescence microscopy and double-helix point spread function optics [Fig. 1(c)] to accumulate 3D spatiotemporal positions of mobile particles [44,45]. 3D trajectories reflected the internal structural geometry of the inverse opal and provided evidence of escape events not generally possible from 2D projections [Figs. 1(d), S10].

To provide an overview of the diffusive behavior, we calculated the equivalent one-dimensional ensemble-average mean-squared displacement (MSD). For nanoparticles dispersed in a bulk liquid, the MSD grew linearly with τ, as expected for Brownian motion, yielding a diffusion coefficient $D = 0.12 \pm 0.01$ μm^2/s over a wide range of timescales. In contrast, the confined diffusion exhibited a classic MSD three-regime behavior associated with cage dynamics [Fig. 2(a)] [46].

For short lag times, the MSD grew linearly with τ, with an effective confined diffusion coefficient, $D_{\text{confined}} = \text{MSD}/2\tau \approx 0.04$ μm^2/s, that was significantly slower than that in bulk liquid. The ensemble-averaged displacement probability distribution in this time regime deviated only slightly from Gaussian behavior [Fig. 2(b)]. We calculated the velocity autocorrelation function (VACF) and found negative values of VACF for lag times in the range $0.1\text{ s} < \tau < 0.3\text{ s}$ [Fig. 2(c)]. Interestingly, the anticorrelation vanished at $\tau \approx 0.3$ s, consistent phenomenologically with the spatially dependent "diffusing diffusivity" model [47–49], arising from particle-wall interactions [50]. This caused a gradual decrease in mobility as a function of proximity to the wall [Fig. 2(d)].

At intermediate lag times, the MSD plot curved downward, sometimes exhibiting an actual plateau due to transient trapping within a cavity for a probabilistic sojourn time. In the longtime limit, a particle escaped a given cavity and hopped among different cages, giving rise to an approximately diffusive behavior, consistent with the cage dynamics in a transient network [51,52]. The ratio of the hole diameter to the tracer particle diameter was expected to have a major impact on the frequency of escape associated with the onset of the longtime regime [Fig. 2(a)]. The effective tracer particle diameter was 48 nm. The hole diameter L for a given inverse opal sample, was determined by analyzing scanning electron microscope images [32,34,44,53–61].

The key quantity required to characterize the narrow escape problem is the sojourn time. For example, the mean

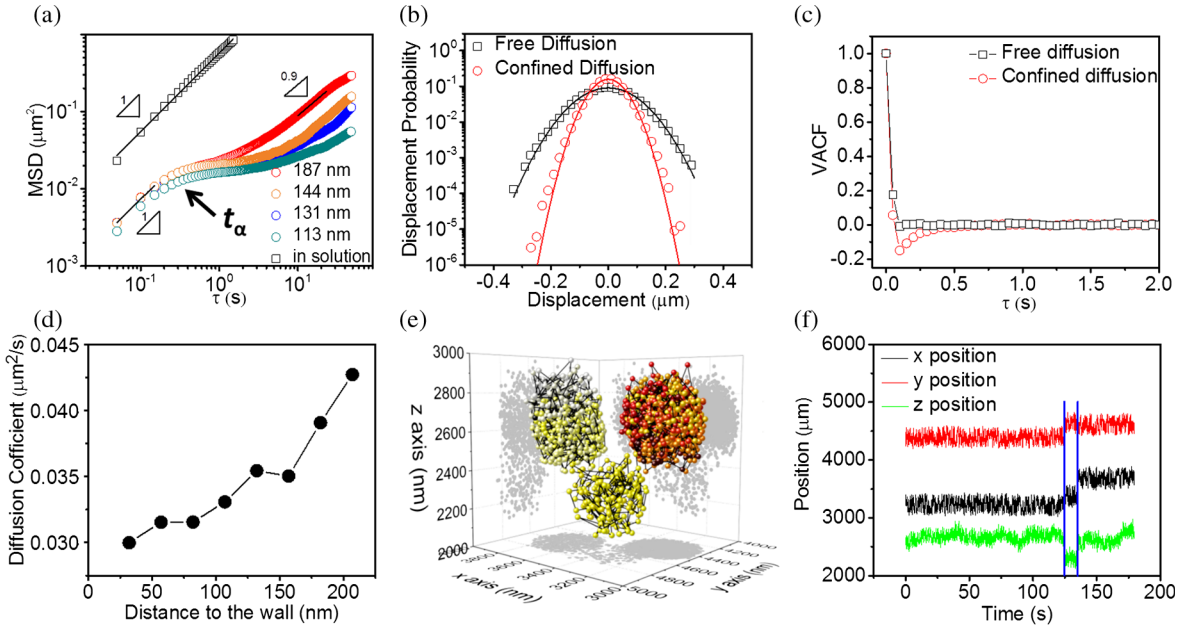

FIG. 2. (a) Plots of MSD versus lag time τ for free diffusion (black square) and confined diffusion at different L (hole diameter). (b) Representative displacement probability distributions for free and confined diffusion at $\tau = 0.05$ s. (c) Representative VACF for free and confined diffusion. (d) Spatially dependent diffusion coefficient as a function of the distance to the wall. (e) Representative trajectory passing through three cavities. (f) Cartesian coordinates of the trajectory from panel (e) as a function of time. The vertical blue lines represent escape events.

sojourn time T_{soj} can be theoretically related to the long-time diffusion coefficient $D_{long} = R^2/6T_{soj}$. To determine these time intervals, we identified the escape from one cavity to another by monitoring the 3D position fluctuation using a maximum allowed displacement approach [Figs. 2(e), 2(f)] [53]. Figure 3(a) shows complementary cumulative distributions of sojourn time in inverse opals at varying L. Because of technical limitations, we obtained reliable and statistically meaningful measurements of T_{soj}, only for L in the range 113–187 nm; T_{soj} was inaccessibly long for $L < 113$ nm (i.e., particles rarely escaped a cavity) despite the fact that the hole diameter was more than twice that of the particle. The distribution of sojourn times was adequately described by the single exponential decay $P(t) = \exp(-t/T_{soj})$, suggesting that the escape was governed by a rate process with a barrier [62]. We found that T_{soj} decreased rapidly with increasing L. For example, as L was increased by a factor of 1.6, T_{soj} decreased more than 4×. This scenario indicates that tightening the escape pathway can effectively decrease the probability of escape [Fig. 3(b)].

To understand the mechanisms controlling the cavity escape process, we performed several calculations to model and interpret the sojourn time distribution. First, from the perspective of short-time diffusion, the time t_α required for a particle to reach the boundary of a cavity of size R can be estimated as $t_\alpha = R^2/6D_{confined} \approx 0.23$ s [Fig. 2(a)]. However, the calculated t_α was nearly 2 orders of magnitude shorter than the minimum measured value of T_{soj}, suggesting that the cavity escape time was much longer than the cavity exploration time. To evaluate this diffusion-limited process quantitatively, we applied two different asymptotic formulas to calculate the MFPT of pointlike particles to reach multiple openings on a cavity, as shown in Figs. 3(b) and S8 [32,34,53]. All parameters used in these calculations were experimentally measured. These two calculations agreed reasonably well with each other and showed a similar trend as experimental measurements, but underestimated the absolute measured sojourn times by a factor of ~20.

In principle, slow particle translocation can arise from factors such as size exclusion, hydrodynamic effects, or long-range interactions between walls and particles. As detailed in the Supplemental Material [53], computer simulations were performed to determine which factors contributed to the measured phenomena [53]. To isolate size-exclusion effects, we performed a kinetic random-walk (RW) simulation to mimic the escape of a finite-size spherical particle from an inverse opal cavity. The RW simulation yielded improved agreement, but still significantly underestimated the measured sojourn times [Fig. 3(b)]. The RW simulation agreed with a standard Brownian dynamics simulation for the calculation of the sojourn time prior to escape [53], suggesting that size-exclusion (entropic) effects cannot solely explain the slow escape. Since the RW simulation did not consider localized hydrodynamic effects [22,23], we performed simulations using modified multiparticle collision dynamics (MPCD)

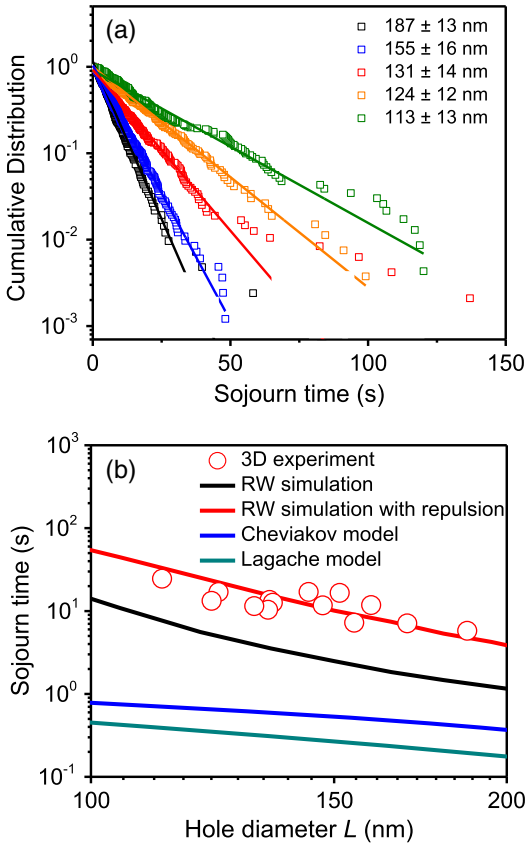

FIG. 3. (a) Cumulative distribution of sojourn times at different L. (b) Sojourn time as a function of L. The circle symbols represent the experimental results. The black and red lines denote simulated results from a RW simulation and a RW simulation involving a repulsive particle-wall potential while the blue and green lines represent theoretical results calculated using the Cheviakov and Lagache models, respectively.

to include momentum exchange between the particle and cavity walls. However, the MPCD results predicted only modestly longer sojourn times, ~20% longer than the predictions of Brownian dynamics simulations under the same conditions (Fig. S11).

Additional control experiments were performed to control and probe the relevance of repulsive particle-wall interactions, by tracking the escape of tracer nanoparticles in an inverse opal film ($L = 150$ nm) that was immersed in a water-glycerol mixture (1:9 by weight). In this aqueous system, the electrostatic repulsion was well defined and could be controlled by changing the salt (NaCl) concentration. When the salt concentration was decreased from $0.1M$ to $0.001M$, corresponding to an increase in the Debye length from 0.96 to 9.6 nm, the mean sojourn time increased from 2.6 to 9.4 s (Fig. S12). Importantly, the sojourn time for the higher-salt system was consistent with the RW simulation result, indicating that the escape is adequately described by the size-exclusion (entropic) effects alone when the electrostatic interaction is screened [19]. Under lower-salt conditions, however, escape was significantly slower, consistent with the observations in Fig. 3(b), suggesting that the slow particle translocation indeed originated from the presence of repulsive particle-wall interactions.

These interactions were further evaluated by considering the radial probability distribution of confined particles (Fig. S13) [50], which exhibited apparent repulsion from cavity walls compared to RW simulations. By considering the types of interactions that may be relevant for nanoparticles in porous media (Table S1) [53], we found that the repulsion was phenomenologically consistent with Coulombic effects in nonaqueous solutions [63,64] or with dipole interactions for objects having large dipole moments in a medium with small dielectric constant [65]. Such a force can provide an additional barrier to escape, that would increase T_{soj} as predicted recently by the Grebenkov-Oshanin model [26].

Since the effects of screening in nonaqueous solution are unclear, the RW simulation was simply modified to include a hypothetical repulsive potential A_{rep} to represent the dipole-dipole interaction between particle and wall, which biases the probabilities of steps towards or away from the cavity walls. In particular, the probability of moving towards the boundary was given as $P = 0.5\text{-}A_{rep}/(r + r_0)^6$, where r denotes the distance to a wall, and a small intercept r_0 was defined to avoid divergence. The only adjustable parameter was A_{rep}, which controlled the strength of the repulsion, and reduced to Brownian motion in the limit of $A_{rep} = 0$ m. By setting $A_{rep} = 3 \times 10^{-6}$ m, excellent agreement was achieved with experimental observations, further supporting a model [Fig. 3(b)] involving the presence of a barrier when approaching the boundary. This can also be expressed as an effective narrowing of the escape pathway, providing a mechanistic interpretation for previous reports that have hypothesized the presence of a decrease in the "effective" diffusion coefficient [66–68] or an increase in the effective diffusion length [69]. In the limiting case, where the particle diameter approaches that of the hole, escape pathways become vanishingly small. Therefore, if the pore size is heterogeneously distributed as expected for most real-world porous materials, the decreased escape pathway makes some openings impermeable to tracer particles, leading to reduced accessibility of a porous network.

In summary, we used 3D tracking to study the escape of Brownian particles in a uniform liquid-filled inverse opal film. The escape from a given cavity was explicitly quantified by measuring the distribution of sojourn times for particles within cavities by analyzing 3D trajectories in inverse opals. The comparison between experiments and theoretical calculations indicated that escape through the bottleneck was barrier controlled rather than diffusion controlled, leading to a decrease in probability of cavity escape and a stronger size-exclusion effect than expected from nominal pore size alone. These results also highlight

the importance of using the sojourn time or MFPT to analyze stochastic processes in confinement [70,71].

We thank Gleb Oshanin and Olivier Benichou for useful discussions. Primary support for experiments and data analysis was provided by the U.S. Department of Energy, Office of Science, Basic Energy Sciences, under Award No. DE-SC0001854. Additional support for data analysis and simulations was provided to D. W. by the National Natural Science Foundation of China (No. 21873094), International Science and Technology Cooperation Program of Jilin, China (Grant No. 20180414007GH), and Jilin Scientific and Technological Development Program (Grant No. 20180519001JH).

*D. W. and H. W. contributed equally to this work.
†To whom correspondence should be addressed. daniel.schwartz@colorado.edu
‡To whom correspondence should be addressed. jzchen@ciac.ac.cn

[1] A. Einstein, Ann. Phys. (Berlin) **322**, 549 (1905).
[2] M. von Smoluchowski, Ann. Phys. (Berlin) **326**, 756 (1906).
[3] D. S. Novikov, E. Fieremans, J. H. Jensen, and J. A. Helpern, Nat. Phys. **7**, 508 (2011).
[4] P. Mathai, J. A. Liddle, and S. M. Stavis, Appl. Phys. Rev. **3**, 011105 (2016).
[5] F. Babayekhorasani, D. E. Dunstan, R. Krishnamoorti, and J. C. Conrad, Soft Matter **12**, 8407 (2016).
[6] I. Y. Wong, M. L. Gardel, D. R. Reichman, E. R. Weeks, M. T. Valentine, A. R. Bausch, and D. A. Weitz, Phys. Rev. Lett. **92**, 178101 (2004).
[7] A. Zurner, J. Kirstein, M. Doblinger, C. Brauchle, and T. Bein, Nature (London) **450**, 705 (2007).
[8] J. Kirstein, B. Platschek, C. Jung, R. Brown, T. Bein, and C. Brauchle, Nat. Mater. **6**, 303 (2007).
[9] Y. Liao, S. K. Yang, K. Koh, A. J. Matzger, and J. S. Biteen, Nano Lett. **12**, 3080 (2012).
[10] D. S. Novikov, J. H. Jensen, J. A. Helpern, and E. Fieremans, Proc. Natl. Acad. Sci. U.S.A. **111**, 5088 (2014).
[11] L. Kisley, R. Brunetti, L. J. Tauzin, B. Shuang, X. Y. Yi, A. W. Kirkeminde, D. A. Higgins, S. Weiss, and C. F. Landes, ACS Nano **9**, 9158 (2015).
[12] D. R. Sapkota, K. H. Tran-Ba, T. Elwell-Cuddy, D. A. Higgins, and T. Ito, J. Phys. Chem. B **120**, 12177 (2016).
[13] K. Hormann, V. Baranau, D. Hlushkou, A. Hoeltzel, and U. Tallarek, New J. Chem. **40**, 4187 (2016).
[14] L. Jiang and S. Granick, ACS Nano **11**, 204 (2017).
[15] V. G. Guimaraes, H. V. Ribeiro, Q. Li, L. R. Evangelista, E. K. Lenzi, and R. S. Zola, Soft Matter **11**, 1658 (2015).
[16] S. J. de Carvalho, R. Metzler, and A. G. Cherstvy, Soft Matter **11**, 4430 (2015).
[17] G. L. Hunter, K. V. Edmond, and E. R. Weeks, Phys. Rev. Lett. **112**, 218302 (2014).
[18] Q. Niu and D. Wang, Curr. Opin. Colloid Interface Sci. **39**, 162 (2019).
[19] P. S. Burada, P. Hanggi, F. Marchesoni, G. Schmid, and P. Talkner, ChemPhysChem **10**, 45 (2009).
[20] D. Nykypanchuk, H. H. Strey, and D. A. Hoagland, Science **297**, 987 (2002).
[21] S. L. Dettmer, S. Pagliara, K. Misiunas, and U. F. Keyser, Phys. Rev. E **89**, 062305 (2014).
[22] X. Yang, C. Liu, Y. Li, F. Marchesoni, P. Hanggi, and H. P. Zhang, Proc. Natl. Acad. Sci. U.S.A. **114**, 9564 (2017).
[23] M. J. Skaug, L. Wang, Y. F. Ding, and D. K. Schwartz, ACS Nano **9**, 2148 (2015).
[24] D. Hlushkou, A. Svidrytski, and U. Tallarek, J. Phys. Chem. C **121**, 8416 (2017).
[25] S. Han, T. M. Hermans, P. E. Fuller, Y. Wei, and B. A. Grzybowski, Angew. Chem. Int. Ed. **124**, 2716 (2012).
[26] D. S. Grebenkov and G. Oshanin, Phys. Chem. Chem. Phys. **19**, 2723 (2017).
[27] O. Benichou and R. Voituriez, Phys. Rev. Lett. **100**, 168105 (2008).
[28] T. Agranov and B. Meerson, Phys. Rev. Lett. **120**, 120601 (2018).
[29] A. Singer, Z. Schuss, D. Holcman, and R. S. Eisenberg, J. Stat. Phys. **122**, 437 (2006).
[30] Z. Schuss, A. Singer, and D. Holcman, Proc. Natl. Acad. Sci. U.S.A. **104**, 16098 (2007).
[31] D. Holcman, N. Hoze, and Z. Schuss, Phys. Rev. E **84**, 021906 (2011).
[32] A. F. Cheviakov, M. J. Ward, and R. Straube, Multiscale Model. Simul. **8**, 836 (2010).
[33] D. S. Grebenkov, Phys. Rev. Lett. **117**, 260201 (2016).
[34] T. Lagache and D. Holcman, J. Stat. Phys. **166**, 244 (2017).
[35] D. Holcman and Z. Schuss, J. Stat. Phys. **117**, 975 (2004).
[36] C. Chevalier, O. Benichou, B. Meyer, and R. Voituriez, J. Phys. A **44**, 025002 (2011).
[37] G. Oshanin, M. Tamm, and O. Vasilyev, J. Chem. Phys. **132**, 235101 (2010).
[38] D. S. Grebenkov and J. F. Rupprecht, J. Chem. Phys. **146**, 084106 (2017).
[39] D. Pedone, M. Langecker, G. Abstreiter, and U. Rant, Nano Lett. **11**, 1561 (2011).
[40] B. Hatton, L. Mishchenko, S. Davis, K. H. Sandhage, and J. Aizenberg, Proc. Natl. Acad. Sci. U.S.A. **107**, 10354 (2010).
[41] R. Raccis, A. Nikoubashman, M. Retsch, U. Jonas, K. Koynov, H. J. Butt, C. N. Likos, and G. Fytas, ACS Nano **5**, 4607 (2011).
[42] S. M. Stavis, J. A. Fagan, M. Stopa, and J. A. Liddle, ACS Appl. Nano Mater. **1**, 4358 (2018).
[43] D. G. Mullen and M. M. Banaszak Holl, Acc. Chem. Res. **44**, 1135 (2011).
[44] D. Wang, A. Agrawal, R. Piestun, and D. K. Schwartz, Appl. Phys. Lett. **110**, 211107 (2017).
[45] D. P. Wang, H. C. Wu, and D. K. Schwartz, Phys. Rev. Lett. **119**, 268001 (2017).
[46] D. Schneider, D. Mehlhorn, P. Zeigermann, J. Karger, and R. Valiullin, Chem. Soc. Rev. **45**, 3439 (2016).
[47] A. V. Chechkin, F. Seno, R. Metzler, and I. M. Sokolov, Phys. Rev. X **7**, 021002 (2017).
[48] A. G. Cherstvy, A. V. Chechkin, and R. Metzler, New J. Phys. **15**, 083039 (2013).
[49] H. B. Eral, J. M. Oh, D. van den Ende, F. Mugele, and M. H. Duits, Langmuir **26**, 16722 (2010).

[50] M. Matse, M. V. Chubynsky, and J. Bechhoefer, Phys. Rev. E **96**, 042604 (2017).
[51] C. Scalliet, A. Gnoli, A. Puglisi, and A. Vulpiani, Phys. Rev. Lett. **114**, 198001 (2015).
[52] S. K. Ghosh, A. G. Cherstvy, and R. Metzler, Phys. Chem. Chem. Phys. **17**, 1847 (2015).
[53] See the Supplemental Material at http://link.aps.org/supplemental/10.1103/PhysRevLett.123.118002 for details of the sample preparation, technique description, analysis methods, and simulation procedure, which includes Refs. [54–61].
[54] S. R. P. Pavani, M. A. Thompson, J. S. Biteen, S. J. Lord, N. Liu, R. J. Twieg, R. Piestun, and W. E. Moerner, Proc. Natl. Acad. Sci. U.S.A. **106**, 2995 (2009).
[55] A. Malevanets and R. Kapral, J. Chem. Phys. **110**, 8605 (1999).
[56] R. G. Winkler, M. Ripoll, K. Mussawisade, and G. Gompper, Comput. Phys. Commun. **169**, 326 (2005).
[57] Y. G. Tao, I. O. Goetze, and G. Gompper, J. Chem. Phys. **128**, 144902 (2008).
[58] T. Ihle and D. M. Kroll, Phys. Rev. E **63**, 020201(R) (2001).
[59] A. Malevanets and R. Kapral, J. Chem. Phys. **112**, 7260 (2000).
[60] C. C. Huang, A. Chatterji, G. Sutmann, G. Gompper, and R. G. Winkler, J. Comput. Phys. **229**, 168 (2010).
[61] J. T. Padding and A. A. Louis, Phys. Rev. E **74**, 031402 (2006).
[62] H. X. Zhou and R. Zwanzig, J. Chem. Phys. **94**, 6147 (1991).
[63] M. F. Hsu, E. R. Dufresne, and D. A. Weitz, Langmuir **21**, 4881 (2005).
[64] C. E. Espinosa, Q. Guo, V. Singh, and S. H. Behrens, Langmuir **26**, 16941 (2010).
[65] C. Shi, B. Yan, L. Xie, L. Zhang, J. Wang, A. Takahara, and H. Zeng, Angew. Chem., Int. Ed. Engl. **55**, 15017 (2016).
[66] J. Xie, M. Doroshenko, U. Jonas, H.-J. Butt, and K. Koynov, ACS Macro Lett. **5**, 190 (2016).
[67] A. Galarneau, F. Guenneau, A. Gedeon, D. Mereib, J. Rodriguez, F. Fajula, and B. Coasne, J. Phys. Chem. C **120**, 1562 (2016).
[68] S.-J. Reich, A. Svidrytski, A. Hoeltzel, J. Florek, F. Kleitz, W. Wang, C. Kuebel, D. Hlushkou, and U. Tallarek, J. Phys. Chem. C **122**, 12350 (2018).
[69] V. Vattipalli, X. Qi, P. J. Dauenhauer, and W. Fan, Chem. Mater. **28**, 7852 (2016).
[70] S. Condamin, O. Benichou, V. Tejedor, R. Voituriez, and J. Klafter, Nature (London) **450**, 77 (2007).
[71] T. Guerin, N. Levernier, O. Benichou, and R. Voituriez, Nature (London) **534**, 356 (2016).